APPLIED PHYSICS LETTERS **107**, 132104 (2015)

Quantum cascade emission in the III-nitride material system designed with effective interface grading

Alex Y. Song,[1,a)] Rajaram Bhat,[2] Andrew A. Allerman,[3] Jie Wang,[2] Tzu-Yung Huang,[1] Chung-En Zah,[1] and Claire F. Gmachl[1]

[1]*Department of Electrical Engineering, Princeton University, Princeton, New Jersey 08540, USA*
[2]*Corning Incorporated, Corning, New York 14831, USA*
[3]*Sandia National Laboratories, Albuquerque, New Mexico 87185, USA*

(Received 15 July 2015; accepted 18 September 2015; published online 29 September 2015)

We report the realization of quantum cascade (QC) light emission in the III-nitride material system, designed with effective interface grading (EIG). EIG induces a continuous transition between wells and barriers in the quantum confinement, which alters the eigenstate system and even delocalizes the states with higher energy. Fully transverse-magnetic spontaneous emission is observed from the fabricated III-nitride QC structure, with a center wavelength of $\sim$4.9 μm and a full width at half maximum of $\sim$110 meV, both in excellent agreement with theoretical predictions. A multi-peak photo-response spectrum is also measured from the QC structure, which again agrees well with theoretical calculations and verifies the effects of EIG.
[http://dx.doi.org/10.1063/1.4932068]

Both the studies of the III-nitride materials[1–3] and the quantum cascade (QC) principle[4–6] have achieved remarkable successes in applications such as light sources and detectors. The merging of the two as III-nitride QC devices has been at the center of research focus for many years.[7–11] Thanks to the many merits of the III-nitride material system including large conduction band offsets ($>$1 eV), high longitudinal optical (LO) phonon energy (up to 99 meV) and high thermal conductivity (up to 2.85 W/cm·K), this bridging is expected to overcome various limitations in traditional devices operating in the mid-IR and terahertz (THz) regions. For example, the spectral regions of 1–2.5 μm and 25–60 μm have been difficult to reach so far.[12–14] Furthermore, room temperature QC operation has not been realized in many sections of the spectrum especially the THz.[15] However, despite the substantial progress in III-nitride QC detectors in the past few years,[8] spontaneous photon emission in III-nitride QC structures seems ever elusive, with the few preliminary results lacking a close connection between the trial designs and actual experimental results.[16,17] This significant discrepancy suggest that our current understanding of the subband structure in the III-nitride material system is incomplete.

In this work, we demonstrate QC light emission from GaN/$Al_xGa_{1-x}N$ superlattices (SLs), which is enabled with theoretical modelling of the III-nitride quantum structure with three-dimensional (3D) interface roughness (IFR). Specific to SLs in III-nitride materials as compared to those in traditional materials like III-arsenide, IFR is found significant and even comparable to the layer thicknesses.[8,18] To characterize properties of III-nitride heterostructures with strong IFR, we have recently developed a theoretical formalism with the help of non-equilibrium Green's functions (NEGF),[19–21] and the results are adopted here. It was shown that with the drop in traditional 2D approximation,[22,23] the first order configurational averaging[24] of the IFR random potential universally gives rise to effective interface grading (EIG). EIG induces continuous transitions between barriers and wells in the band diagram and dramatically changes the wave functions and energy spectrum of the SLs. Here, we fully integrate EIG in to the QC structure design. IFR scattering was also remodelled with the 3D IFR stochastic potential, where the Feynman diagrams of the scattering self-energy are calculated in the self-consistent Born Approximation (SCBA).[20] The resulting ultra-strong intersubband (ISB) IFR scattering is dominant over LO phonon scattering and is employed here to facilitate charge transport in the SLs. Also intrinsic to III-nitride heterostructures are the non-linear spontaneous and piezoelectric polarizations, which are calculated *in-situ* with dependence on local strain in each layer, and added to the superlattice potential.[25,26] The electron-electron and electron-ionized impurity interactions are treated within the mean-field approximation, i.e., the Poisson equation, and is calculated self-consistently until the band structure converges. With this step, the electric potential arising from charge re-distribution is included.

The III-nitride QC structure is grown by metalorganic chemical vapor deposition (MOCVD) on sapphire. Complex template layers are employed to release the strain and ensure flat surface morphology. The bottom contact layer, the active QC emitter layers, and the top contact layer are grown consecutively on top of the template. The bottom and the top contact layers are bulk $Al_{0.26}Ga_{0.74}N$ with thicknesses of 600 nm and 150 nm, respectively. They are doped with Si to a level of $1 \times 10^{19}\,cm^{-3}$. The epi-layers are relaxation-free with a surface roughness ≤ 5 Å. Round mesa devices are fabricated for spectral measurements. The mesas are processed by inductively coupled plasma (ICP) reactive ion etching. Contact metallization of Ti 6 nm/Al 180 nm/Ni 55 nm/Au 300 nm is carried out in an electron-beam evaporator. The samples are then annealed at 800 °C for 80 s. Spectral characterizations are performed with the Fourier Transform Infrared Spectrometer (FTIR).

a)alexys@stanford.edu

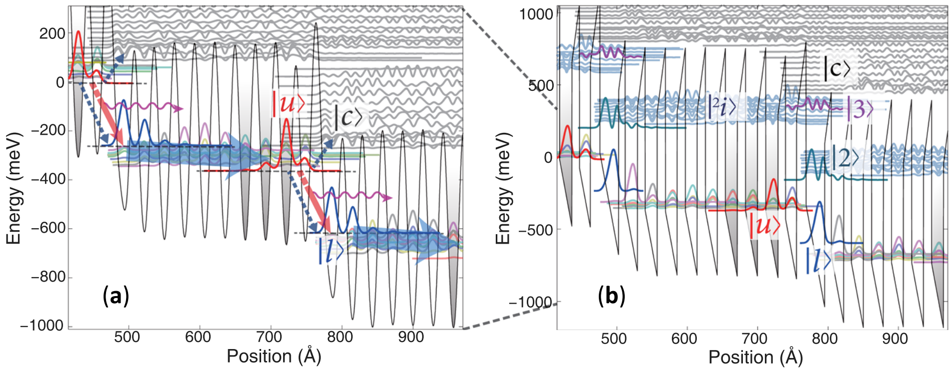

FIG. 1. Band structure of the III-nitride QC emitter. (a) Band structure calculated with EIG. The structure features a diagonal optical transition at 4.9 μm (red arrows). $|u\rangle$, $|l\rangle$, and $|c\rangle$ are the upper emitter state, the lower emitter state, and the continuum, respectively. The thick blue arrows indicate the direction of carrier flow. Non-radiative leakage paths are indicated in the dashed blue arrows. The applied bias is 120 kV/cm. Si doping of $1.8\times10^{18}\,\mathrm{cm}^{-3}$ is introduced in the shaded quantum wells. Growth direction: left to right. (b) Band structure calculated without EIG. States $|2\rangle$, $|3\rangle$, and the manifold $|^2i\rangle$ are confined, all of which are absent in the actual band structure in (a). Note the significantly larger energy range than in (a).

The band structure of the III-nitride QC emitter studied in this work is shown in Fig. 1(a). An IFR height of 5 Å and an IFR correlation length of 10 Å are assumed in the band structure design. These IFR parameters are estimated based on our previous study of the IFR effects in III-nitride SLs, where they explain the experimentally observed eigenenergy shifts and states broadening.[21] Two material compositions are employed in the QC layers, i.e., GaN as wells and $Al_{0.65}Ga_{0.35}N$ as barriers. The emitter is comprised of 50 periods of the QC structure, with each period containing 10 quantum wells. The nominal layer thicknesses in one period are 11.7/**16.7**/11.8/**16.8**/11.6/**16.8**/11.8/**16.8**/11.9/**17.4**/10.7/**15.6**/13.5/**26.5**/9.4/**17.5**/11/**17**/11.8/**16.6** in units of Angstroms, where bold numbers indicate GaN wells. The underlined layers are doped with Si to a level of $1.8\times10^{18}\,\mathrm{cm}^{-3}$. The QC emitter features a diagonal optical transition centered at 4.9 μm ($\sim$255 meV). The calculated full width at half maximum (FWHM) of the optical transition is 90 meV taking into account both the IFR and LO phonon scattering.[27,28] Here, varying the correlation length of IFR by $\pm$2 Å would modify the FWHM by $\pm$30 meV.

It is important to understand the nature of carrier transport in III-nitride SLs[29] and design it in favor of QC operation. To this end, we have calculated the scattering lifetimes in the relevant transport channels of the QC structure, which are listed in Table I. As is shown, both LO phonon scattering and IFR scattering are strong between the injector states, in carrier injection $|i\rangle\rightarrow|u\rangle$ and in carrier extraction $|l\rangle\rightarrow|i\rangle$. IFR scattering is especially fast due to significant IFR in this material system. The leakage into continuum $|u\rangle\rightarrow|c\rangle$ is kept small with the large energy difference between the upper emitter state $|u\rangle$ and the continuum states $|c\rangle$ of $\geq$100 meV. Consequently, carrier transport among injector states (including carrier injection/extraction) is $>10^2$ times more efficient than the non-radiative leakage from $|u\rangle$ to $|l\rangle$ or $|c\rangle$. This favors the carrier accumulation on the upper emitter level and is ideal for light emission. The calculated impurity scattering lifetimes are $\geq$50 ns,[24] which is considerably slower than LO phonon interactions or IFR scattering.

TABLE I. Calculated scattering lifetimes at 300 K in different transport channels of the III-nitride QC emitter. $|u\rangle$, $|l\rangle$, $|i\rangle$, $|c\rangle$ stand for the upper emitter state, the lower emitter state, the injector states, and the continuum states, respectively. $|i\rangle\rightarrow|i\rangle$ is the typical value from one injector state to all the others.

Channel	LO scattering (ps)	IFR scattering (ps)
$\|u\rangle\rightarrow\|l\rangle$	5.9	2.6
$\|i\rangle\rightarrow\|i\rangle$	0.047	0.016
$\|l\rangle\rightarrow\|i\rangle$	0.055	0.039
$\|i\rangle\rightarrow\|u\rangle$	0.045	0.024
$\|u\rangle\rightarrow\|c\rangle$	17	2.5

As is seen in Fig. 1(a), EIG manifests itself strongly in the band structure. For a comparison, the band structure without EIG is shown in Fig. 1(b). It is clear that EIG dramatically changes the shape of the quantum wells and make them far less deep, which is followed by significant alternations in both the wave functions and the eigenenergy spectrum. For example, state $|2\rangle$, manifold $|^2i\rangle$, and state $|3\rangle$ have all vanished into continuum with the inclusion of EIG. The energy spacing between $|u\rangle$ and the continuum in Fig. 1(b) is as large as $\sim$0.8 eV, with only 0.1 eV in the actual band structure in Fig. 1(a). Furthermore, the optical transition between $|u\rangle$ and $|l\rangle$ in Fig. 1(b) is at 5.6 μm instead of 4.9 μm as in Fig. 1(a).

Spontaneous light emission is realized in the designed III-nitride QC emitter. The emission spectra are shown in Fig. 2. For this measurement, the QC device is electrically pumped with a bias field of 120 kV/cm and a current density of 3.2 kA/cm^2 in the pulsed mode. The repetition rate is 110 kHz with a duty cycle of 1.3%. As is shown in Fig. 2, the designed QC light emission is observed with a center wavelength of 4.9 μm. In the low energy region below 200 meV, the heat radiation is also observed in both of the transverse magnetic (TM) and the transverse electric (TE) spectra. The heat radiation is unpolarized; thus, for an authentic comparison, we normalize the spectra in the two polarizations to the heat peak. Comparing the TM and TE spectra at 80 K, it is clear that the QC emission is only observed in the TM polarization, verifying its origin in the ISB transitions. The peak transition wavelength of 4.9 μm ($\sim$255 meV) is in excellent agreement with the design. The FWHM of the emission is about 110 meV, which also agrees well with the calculation. The QC emission peak is weaker

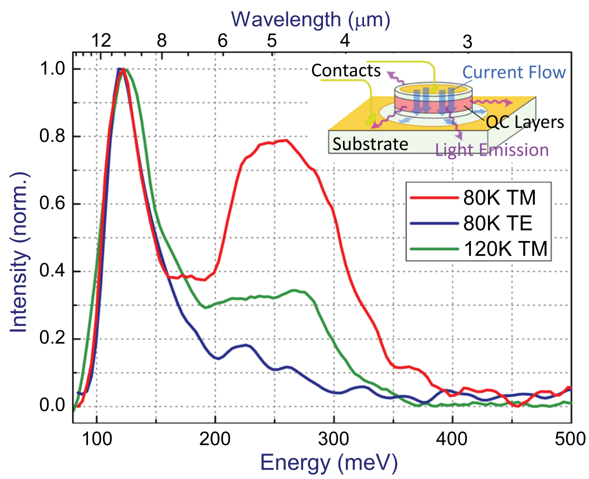

FIG. 2. Emission spectra of the III-nitride QC emitter. Red: TM emission at 80 K. Blue: TE emission at 80 K. Green: TM emission at 120 K. The QC light emission is observed in the TM spectra at around 255 meV. Unpolarized heat radiation is observed below 200 meV. Inset: schematic of the mesa device.

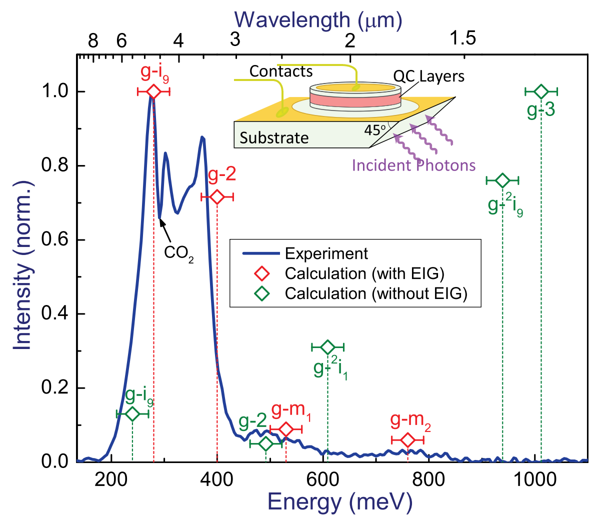

FIG. 4. Photocurrent spectra of the III-nitride QC emitter. Strong peaks are observed at about 280 meV and 380 meV. In the higher energy region, two weak and broad peaks centered at ∼520 meV and ∼770 meV are also discernable. The predicted peak positions from the calculation with and without EIG are marked in the red and green diamonds, respectively. The measurement is performed at 80 K. Inset: schematic of the processed mesa device and light incidence.

at 120 K compared to 80 K, but is still clearly observable above the TE background. The observed light emission is repeatable across multiple sample growths.

The effects of EIG in the band diagram can be verified by the photo-response characteristics of the structure. The III-nitride QC emitter studied here doubles as a QC photodetector at zero external bias, and the calculated band diagrams with and without EIG are shown in Figs. 3(a) and 3(b), respectively. The measured photo-response spectrum of the structure is plotted in Fig. 4.

Comparing Figs. 3(a) and 3(b), it is again clear that inclusion of EIG significantly changes the band diagram. Multiple optical absorption paths can be found in Fig. 3(a): from the ground state $|g\rangle$ to $|i_9\rangle$, $|2\rangle$, $|m_1\rangle$, and $|m_2\rangle$, respectively. The states in the manifold $|m_1\rangle$ are grouped, since the energy spacing between them is small (<50 meV), which is comparable to the estimated broadening of each state (>40 meV). For the same reason, we group the manifold $|m_2\rangle$. Each of the four optical transitions shown in Fig. 3(a) is expected to induce a photocurrent response at the corresponding photon energy, which is indicated in Fig. 4 (red markers). The calculated peak energies of these transitions are 280 meV, 400 meV, 530 meV, and 760 meV, respectively, with an estimated uncertainty of ±30 meV from a variation in the IFR height of ±0.5 Å. The relative strength of the photo-response peaks are estimated based on the escape probabilities and the dipole matrix elements.[11] As shown in Fig. 4, this calculation with EIG agrees very well with the measured spectrum. In comparison, the expected photo-response peaks corresponding to the traditional band structure without EIG in Fig. 3(b) are also indicated in Fig. 4 (green markers). It is clear that in this case the calculation results do not match the experimental observation at all. For example, the predicted transition $|g\rangle \rightarrow |3\rangle$ at around 900 meV is not observed experimentally. This is because $|3\rangle$ is absent in the actual band structure.

In conclusion, we have realized III-nitride QC emission in the mid-IR, enabled by employing EIG in the quantum structure design. We show that EIG is an extra degree of freedom in the quantum design; it breaks the classical picture

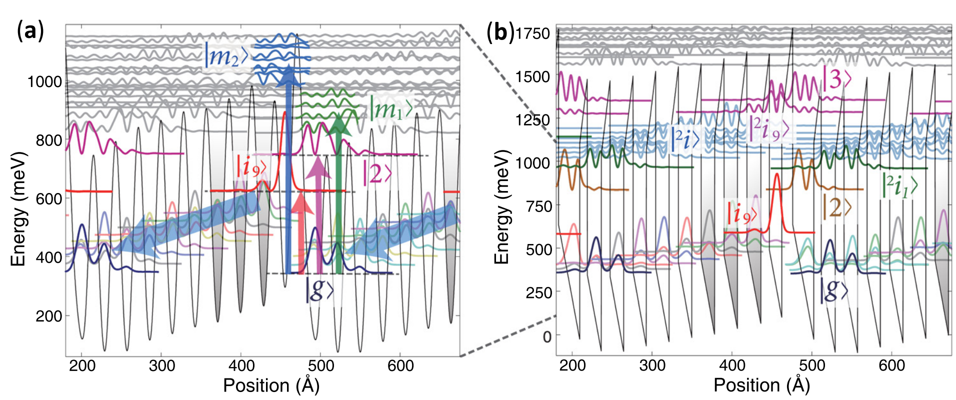

FIG. 3. Band diagram of the III-nitride QC structure without external bias. (a) Band structure calculated with EIG. Optical transitions from $|g\rangle$ to $|i_9\rangle$, $|2\rangle$, $|m_1\rangle$, and $|m_2\rangle$ are marked with arrows in different colors. The direction of electron flow is indicated in the thick blue arrow. (b) Band structure calculated without EIG. The second confined states in the injector quantum wells are separated from the continuum, and they form the manifold $|^2i\rangle$. Also, state $|3\rangle$ is now well confined, which is absent in the actual band structure in (a). Note the energy scale comparison in (a) compared to (b).

of well-defined quantum wells with vertical barrier walls and dramatically alters the band structure. Aided by EIG, theoretical calculations accurately produce the band diagram of the functional III-nitride QC emitter under study. Ultra-short IFR scattering lifetimes ($\sim$0.02 ps) and LO phonon scattering lifetimes ($\sim$0.05 ps) are employed to facilitate transport in the QC. Spontaneous light emission is observed with a center wavelength of 4.9 μm ($\sim$255 meV) and a FWHM of about 110 meV, both of which in excellent agreement with the theoretical calculation. The work presented in this letter extends the capabilities of III-nitrides to longer wavelength portions of the spectrum. The knowledge gained here also opens up opportunities for quantum design in heterostructures with large interface inhomogeneity.

This work was supported by MIRTHE (EEC-0540382). We thank Dr. Germano Penello for valuable discussions.

[1]S. Pimputkar, J. S. Speck, S. P. DenBaars, and S. Nakamura, Nat. Photonics **3**, 180 (2009).
[2]A. Khan, K. Balakrishnan, and T. Katona, Nat. Photonics **2**, 77 (2008).
[3]H. Morkoc and S. N. Mohammad, Science **267**, 51 (1995).
[4]Y. Yao, A. J. Hoffman, and C. F. Gmachl, Nat. Photonics **6**, 432 (2012).
[5]J. Faist, F. Capasso, D. L. Sivco, C. Sirtori, A. L. Hutchinson, and A. Y. Cho, Science **264**, 553 (1994).
[6]A. Kosterev, G. Wysocki, Y. Bakhirkin, S. So, R. Lewicki, M. Fraser, F. Tittel, and R. Curl, Appl. Phys. B **90**, 165 (2008).
[7]N. Suzuki and N. Iizuka, Jpn. J. Appl. Phys., Part 2 **38**, L363 (1999).
[8]S. Sakr, P. Crozat, D. Gacemi, Y. Kotsar, A. Pesach, P. Quach, N. Isac, M. Tchernycheva, L. Vivien, G. Bahir, E. Monroy, and F. H. Julien, Appl. Phys. Lett. **102**, 011135 (2013).
[9]C. Edmunds, J. Shao, M. Shirazi-HD, M. Manfra, and O. Malis, Appl. Phys. Lett. **105**, 021109 (2014).
[10]E. Bellotti, K. Driscoll, T. D. Moustakas, and R. Paiella, Appl. Phys. Lett. **92**, 101112 (2008).
[11]Y. Song, R. Bhat, T.-Y. Huang, P. Badami, C.-E. Zah, and C. Gmachl, Appl. Phys. Lett. **105**, 182104 (2014).
[12]O. Cathabard, R. Teissier, J. Devenson, J. Moreno, and A. Baranov, Appl. Phys. Lett **96**, 141110 (2010).
[13]R. Colombelli, F. Capasso, C. Gmachl, A. L. Hutchinson, D. L. Sivco, A. Tredicucci, M. C. Wanke, A. M. Sergent, and A. Y. Cho, Appl. Phys. Lett. **78**, 2620 (2001).
[14]M. Kim, C. Canedy, W. Bewley, C. Kim, J. Lindle, J. Abell, I. Vurgaftman, and J. Meyer, Appl. Phys. Lett. **92**, 191100 (2008).
[15]S. Fathololoumi, E. Dupont, C. Chan, Z. Wasilewski, S. Laframboise, D. Ban, A. Mátyás, C. Jirauschek, Q. Hu, and H. Liu, Opt. Express **20**, 3866 (2012).
[16]D. Hofstetter, D. P. Bour, and L. Kirste, Appl. Phys. Lett. **104**, 241107 (2014).
[17]W. Terashima and H. Hirayama, Phys. Status Solidi C **8**, 2302 (2011).
[18]P. Cristea, Y. Fedoryshyn, J. Holzman, F. Robin, H. Jackel, E. Muller, and J. Faist, J. Appl. Phys. **100**, 116104 (2006).
[19]Y. Song, R. Bhat, C.-E. Zah, and C. Gmachl, Bull. Am. Phys. Soc. **59**, BAPS.2014.MAR.L45.11 (2014).
[20]A. Wacker and A.-P. Jauho, Phys. Rev. Lett. **80**, 369 (1998).
[21]A. Y. Song, R. Bhat, P. Bouzi, Z. Chung-En, and C. F. Gmachl, e-print arXiv:1507.06016 [cond-mat].
[22]F. Chevoir and B. Vinter, Phys. Rev. B **47**, 7260 (1993).
[23]J. B. Khurgin, Appl. Phys. Lett. **93**, 091104 (2008).
[24]J. Rammer and H. Smith, Rev. Mod. Phys. **58**, 323 (1986).
[25]F. Bernardini and V. Fiorentini, Phys. Rev. B **64**, 085207 (2001).
[26]M. Miao, Q. Yan, C. Van de Walle, W. Lou, L. Li, and K. Chang, Phys. Rev. Lett. **109**, 186803 (2012).
[27]T. Unuma, M. Yoshita, T. Noda, H. Sakaki, and H. Akiyama, J. Appl. Phys. **93**, 1586 (2003).
[28]T. Ando, A. B. Fowler, and F. Stern, Rev. Mod. Phys. **54**, 437 (1982).
[29]R. C. Iotti and F. Rossi, Phys. Rev. Lett. **87**, 146603 (2001).